JOURNAL OF CATALYSIS 142, 455–464 (1993)

Supported Ternary Sulfide Phases: Characterization and Catalytic Properties of Alumina-Supported $Ni_xRu_{1-x}S_2$

J. A. DE LOS REYES,* M. VRINAT,*,[1] C. GEANTET,* M. BREYSSE,* AND J. GRIMBLOT†

*Institut de Recherches sur la Catalyse, CNRS, 2 avenue Albert Einstein, F-69626 Villeurbanne Cedex, France; and †Laboratoire de Catalyse Hétérogène et Homogène (U.A. CNRS 402), Université des Sciences et Techniques de Lille, Flandres-Artois, F-59655 Villeneuve d'Ascq Cedex, France

Received September 9, 1992; revised February 22, 1993

Mixed nickel–ruthenium sulfides supported over alumina, with different metal compositions, were prepared by stepwise impregnation and further sulfidation. The solids were characterized by XRD, XPS, HREM, STEM, and TPR, and their catalytic properties evaluated using the hydrogenation of biphenyl. XRD, XPS, TPR, and STEM measurements indicate that ternary nickel–ruthenium–sulfur compounds with a pyrite-like structure are synthesized up to an atomic ratio of Ni/(Ni + Ru) near 0.7. STEM analysis after tests shows that these phases are stable under test conditions. A 30-fold increase in hydrogenation activity is observed in comparison to pure ruthenium sulfide supported on alumina. This synergetic effect is ascribed to the existence of mixed NiRu sites with different electronic properties from those of either Ni or Ru sites by themselves.

INTRODUCTION

Conventional alumina-supported CoMo, NiMo, and NiW sulfides have been studied in relation to their hydrotreating properties over the last three decades (*1*). Nowadays, these catalysts are extensively employed in the petroleum processing industry to perform heteroatom removal and hydrogenation reactions. However, recent environmental and economic problems offer a challenge for developing new catalysts capable of deep hydrodesulfurization (HDS) and hydrogenation (HYD) of aromatics in the presence of sulfur and nitrogen compounds.

In the last decade, other transition metal sulfides have been investigated. For example, Pecoraro and Chianelli (*2*) and Lacroix *et al.* (*3*) have reported that unsupported RuS_2 exhibits high hydrodesulphurization and hydrogenation activity. Furthermore, mixed compounds of RuS_2 and other pyrite-type sulfides like RhS_2 (*4*), NiS_2 (*5, 6*), CoS_2 (*4, 6*), or FeS_2 (*6*) were synthesized. For ruthenium-sulfide-based solids, the catalytic performance using thiophene HDS and biphenyl HYD were also determined. Among these new phases, the members of the system $Ni_xRu_{1-x}S_2$ appeared to be the most promising, since their catalytic properties for both types of reactions were found to be higher than those for both RuS_2 and the mixed unsupported NiMo sulfide catalyst (*6*). Consequently, it was of particular interest to examine if such ternary phases can be transposed to the supported state.

Recently, we have reported that such transposition from the unsupported to the supported state was difficult for ruthenium sulfide catalysts due to the importance of the sulfidation step in the genesis of active RuS_2/Al_2O_3 catalysts (*7, 8*). Moreover, the existence of supported ternary sulfide phase has not been previously reported in the literature since in the conventional NiMo catalyst, the nickel atoms are assumed to be located only on the edges of the MoS_2 structure.

[1] To whom correspondence should be addressed.

0021-9517/93 $5.00

Taking into account these previous studies concerning the unsupported ternary pyrite-like phases and ruthenium sulfide supported over alumina, the primary objective of the present work was the preparation and the characterization of $Ni_xRu_{1-x}S_2$ supported over alumina. A secondary objective was to assess the hydrogenation properties of these new catalysts using biphenyl conversion as a model reaction and to compare their performance to those for a typical commercial $NiMo/Al_2O_3$ catalyst.

EXPERIMENTAL

Catalyst Preparation

The $NiRu/Al_2O_3$ catalysts containing 7 wt% of total metal were prepared by incipient wetness impregnation. The catalysts are identified by the atomic ratio r = Ni/(Ni + Ru), which corresponds to the number of Ni atoms impregnated in the catalyst divided by the total number of Ni and Ru atoms in the sample. For the NiRu(0.0) and NiRu(1.0) catalysts, the outgassed carrier was contacted with the appropriate precursor salt solution and then oven dried at 383 K for 16 h. The other $NiRu/Al_2O_3$ catalysts were prepared by a stepwise procedure in which Ru was first deposited by the method described above. The dried Ru/Al_2O_3 catalyst was then impregnated with a solution of the Ni salt by the incipient wetness process, and finally the catalysts were dried at 383 K for 16 h. Calcination was avoided for the Ru-based samples, while the pure nickel catalyst was calcined at 623 K.

$RuCl_3 \cdot 3H_2O$ (Aldrich Chemie) and $NiCl_2$ (Merck) were used as precursor salts while crunched and sieved γAl_2O_3-alumina (0.08–0.12 mm fraction) was employed as a support (BET surface area 236 $m^2 g^{-1}$). The commercial catalyst (14 wt% MoO_3 and 3 wt% NiO supported on Al_2O_3) was provided by Procatalyse.

Prior to the characterization studies and the catalytic tests, the catalysts were sulfided in a flow reactor for 4 h under an N_2/H_2S (15%) mixture once a constant temperature of 873 K was achieved (heating rate 0.16 K s^{-1}). After cooling to room temperature, the reactor was flushed with an N_2 flow, and the samples were stored in sealed bottles under argon in order to preserve the catalysts from oxidation. Ruthenium and nickel compositions of the samples were measured by dissolution in an oxidizing acid and analyzed by atomic absorption spectroscopy. This method for determination of the catalyst composition was utilized for the evaluation of the ratio r that characterized each sample. Sulfur chemical analysis were then performed by coulometric detection.

Reaction Test

The determination of hydrogenation activities was carried out in the vapour phase using a fixed-bed microreactor (SOTELEM RDP 830) operating at total pressure of 2300 kPa and temperature of 530 K, with 43.5 kPa of H_2S and 0.8 kPa of biphenyl added into the H_2 flow.

In order to obtain low biphenyl conversions ($X < 15\%$), the weight of the catalyst charged into the reactor was varied from 0.10 to 0.25 g. The reaction rate was determined after an overnight time on stream according to the equation

$$R_B = F_{B0} \cdot X_B / W_c, \qquad (1)$$

where R_B = reaction rate (mol s^{-1} g^{-1}) of biphenyl consumption, F_{B0} = molar flow rate of biphenyl (mol.s^{-1}), X = conversion, and W_c = weight of catalyst (g). Examination of the conversion versus time on stream indicates that after some deactivation during the first few hours of the run, the pseudo-stationary state is reached after 5 to 6 h.

X-Ray Diffraction

Powder diffraction lines of the catalysts after sulfidation were obtained with a SIEMENS D 500 diffractometer (Cu $K\alpha$ radiation : 0.1542 nm), and their identification was made according to the JCPDS index. For all the samples, a scan of 1° min^{-1} was used and the 2θ range between 10° and 70° was investigated. Pure silicon was employed as an internal standard. The lattice

parameter a of the cubic pyrite structure was calculated according to the least-squares analysis method.

XPS Measurements

XPS experiments were performed in an AEI ES 200 B spectrometer using Al $K\alpha$ radiation. The transfer of the sulfided samples was carried out in a glove-box attached to the spectrometer in the absence of air and moisture. Binding energies (BE) were referenced to Al 2p at 74.8 eV. The signal intensities were measured by using integrated areas under the detected peaks. To evaluate the surface atomic ratios, the following equation was employed,

$$n_1/n_2 = (I_{1x}/I_{2y})(\sigma_{2y}T_{2y}k_{2y})/(\sigma_{1x}T_{1x}k_{1x}), \quad (2)$$

where n_1, n_2 = number of atoms of either element 1 or 2 that was analyzed, I_{1x}, I_{2y} = intensity of a peak, and σ_{1x}, σ_{2y} = cross section, taken from Scofield (*9*), of the core level x or y, for a chosen element 1 or 2. If one assumes that the transmission factor of the spectrometer is proportional to the kinetic energy (KE) and that the mean free path of the photoelectron of a specific level is proportional to $KE^{0.8}$ (*10*), Eq. (2) becomes

$$n_1/n_2 = (I_{1x}/I_{2y})(\sigma_{2y}KE_{2y}^{1.8})/(\sigma_{1x}KE_{1x}^{1.8}). \quad (3)$$

Electron Microscopy

High-resolution electron microscopy examinations were performed with a JEOL 100 CX instrument fitted with a UHP polar piece (resolving power 0.2 nm). The solids were ultrasonically dispersed in ethanol and the suspension was collected on carbon-coated copper grids. STEM analysis was made on a VG HB501 apparatus.

TPR Experiments

The temperature-programmed reduction was carried out in a dynamic microreactor which allowed us to measure the amount of H_2S removed under hydrogen by the use of a specific UV photodetector (HNU photoionisation detector equipped with a 10.21-eV UV light source). The amount of H_2S evolved from the solid is simply quantified by the integration of the UV photodetector signal, after the detector calibration with a known concentration of hydrogen sulfide diluted in hydrogen. At the beginning of the experiment the sample was first flushed with a nitrogen flow until no H_2S was detected and then contacted with a H_2 flow of 0.65 cm^3/s at room temperature and the temperature raised to 1273 K at a rate of 0.03 K s^{-1}. Details have been reported in previous papers (*11*, *12*).

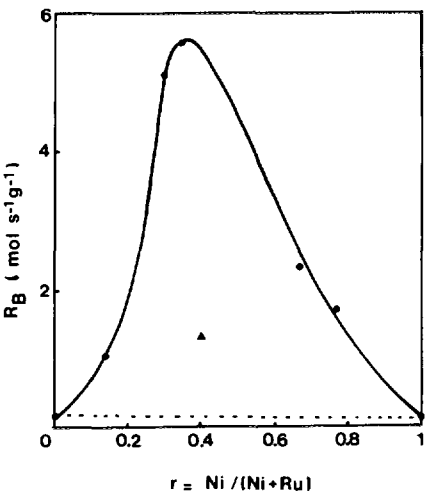

FIG. 1. Evolution of the catalytic properties of NiRu catalysts in biphenyl hydrogenation with the atomic composition r = Ni/(Ni + Ru) (dashed line indicates the sum of the rates displayed by the corresponding amount of pure ruthenium and pure nickel-supported catalysts). (▲) $NiMo/Al_2O_3$ reference catalyst.

RESULTS

Catalytic Activities

The variation of the biphenyl HYD rate, evaluated from Eq. (1), versus the atomic composition r is shown in Fig. 1. The HYD rate sharply increases with r, reaches a maximum between r = 0.35–0.45, and then decreases continuously down to the low value observed for pure nickel sulfide. The maximum of the HYD rate is ca. 30 times higher

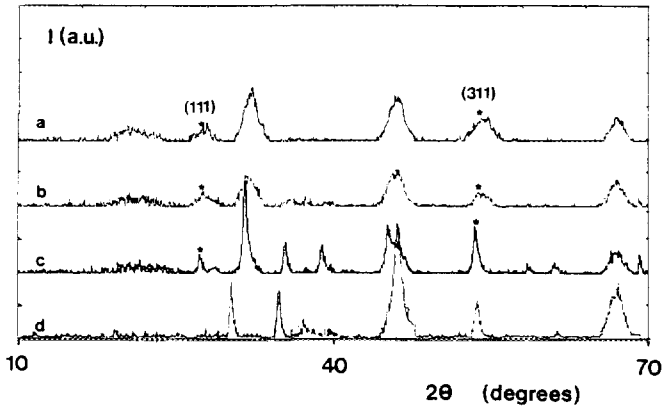

FIG. 2. XRD patterns of the NiRu sulfided samples: (a) NiRu(0.0), (b) NiRu(0.35), (c) NiRu(0.77), and (d) NiRu(1.0). (*) Pyrite-like structure XRD lines.

than the sum of the rates displayed by the corresponding amount of ruthenium and nickel supported sulfides (dashed line in Fig. 1), clearly pointing out a synergetic effect. However, for supported catalysts, this enhancement of the catalytic properties is much higher than for unsupported catalysts which presented only a twofold increase of the activity for $Ni_xRu_{1-x}S_2$ by comparison to RuS_2 (5). In addition, the HYD rate for the supported NiRu(0.35) sample is four times higher than the activity of the commercial Ni–Mo/Al_2O_3 ($A_S = 1.3 \times 10^{-8}$ mol s^{-1} g^{-1}). This reference sample was previously sulfided [H_2/H_2S(15%) at 673 K] and tested under the same conditions as nickel ruthenium catalysts.

X-Ray Diffraction

Some sulfided NiRu/Al_2O_3 samples were examined by X-ray powder diffraction (Fig. 2). For the NiRu samples with $r = 0.0, 0.35$, and 0.7, the XRD patterns are very similar and the lines are attributed to a cubic pyrite structure. For the sample containing only nickel, NiRu(1.0), the X-ray intensity curve differs significantly from the other samples (Fig. 2d), with lines corresponding to an NiS phase, reported in the JCPDS index (2-1280), different of the millerite NiS and which is not a pyrite-type structure. It should be noted that alumina shows scattering angles similar to those of the pyrite structure. Thus, the (111) and (311) reflections of the pyrite structure are only used in order to avoid overlapping caused by the support lines.

In the previous studies concerning unsupported $Ni_xRu_{1-x}S_2$, the XRD patterns were interpreted on the basis of a cubic pyrite structure (5). The lattice parameters were found to verify Vegard's law. This linear change of the cell parameter with the composition is a proof of solid solution formation. Since a cubic pyrite structure is also observed in the present work for the NiRu samples, the lattice parameter a can be calculated for NiRu(0.35) and NiRu(0.7) samples as described earlier. The experimental results (0.562 and 0.568 nm, respectively) are in reasonable agreement with those reported for unsupported $Ni_xRu_{1-x}S_2$ (5) with the same stoichiometry. Thus, it can be inferred that the NiRu catalysts with $r = 0.35$ and 0.7 consist of $Ni_xRu_{1-x}S_2$ solid solutions supported over alumina. The unicomponent catalysts correspond respectively to RuS_2 and NiS.

XPS Spectroscopy

Binding energies for the sulfided NiRu/Al_2O_3 catalysts are summarized in Table 1.

TABLE 1

XPS Data for $NiRu/Al_2O_3$ Sulfided Samples

Sample	Binding energy (eV)			XPS ratios	
	S 2*p*	Ru $3d_{5/2}$	Ni $2p_{3/2}$	Ni/(Ni + Ru)	S/(Ru + Ni)
NiRu(0.00)	163.1	280.0	—	0.00	4.3
NiRu(0.14)	162.7	279.9	853.5	0.18	2.9
NiRu(0.35)	162.8	279.9	853.6	0.43	3.0
NiRu(0.50)	162.8	280.0	853.8	0.46	3.1
NiRu(0.77)	162.4	280.0	853.2	0.63	3.0
NiRu(1.00)	161.3	—	852.4	1.00	3.0

The Ru $3d_{5/2}$ binding energies do not vary throughout the series and can be assigned to Ru^{2+} in ruthenium disulfide (*5*, *13*).

Besides, the S 2*p* and Ni 2*p* spectra recorded for the NiRu catalysts show some modifications depending on the ratio *r*. For the NiRu(0.0) catalyst (see Fig. 3), the main peak in the S 2*p* doublet is ascribed to $(S_2)^{2-}$ species, as reported previously (*7*, *8*). Spectra recorded for samples with *r* up to 0.5 exhibit S 2*p* maxima at a constant BE (162.8 ± 0.1 eV) with 3.1 ± 0.1 eV as full width at half-maximum (FWHM), pointing out disulfide polyanions at the surface. For *r* = 0.77, the BE decreases to 162.4 eV and may indicate the presence of some amount of S^{2-} anions. Then, a peak at 161.3 eV is observed for the pure Ni sample indicating S^{2-} sulfide species.

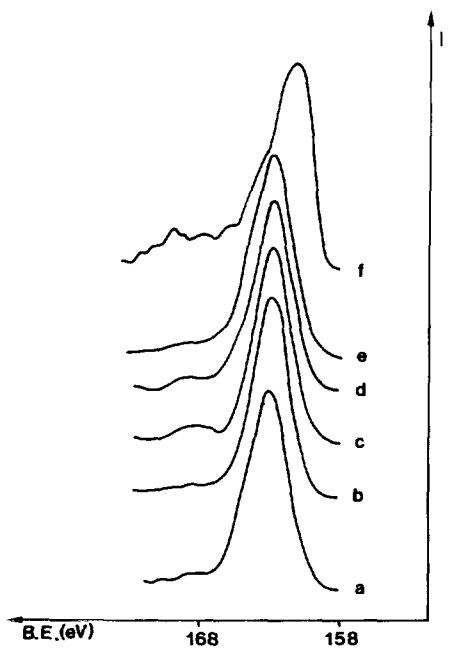

FIG. 3. S $2p_{1/2}$ and S $2p_{3/2}$ spectra of the sulfided catalysts: (a) NiRu(0.0), (b) NiRu(0.14), (c) NiRu(0.35), (d) NiRu(0.50), (e) NiRu(0.77), and (f) NiRu(1.0).

The Ni $2p_{1/2-3/2}$ spectra are given in Fig. 4. In the $0.15 \leq r \leq 0.5$ domain, the Ni $2p_{3/2}$ BE varied between 853.5 and 853.8 eV, consistent with published data for supported nickel sulfides (*14*). The Ni $2p_{3/2}$ BE for the Ru–Ni with *r* = 0.77 and 1.0 samples shift to lower values. This may be due to the larger crystal field splitting in NiS_2 (octahedral coordination of Ni) different from that of NiS (five sulfur neighbours in the millerite structure, for example).

The atomic nNi/(nRu + nNi) ratios calculated from the XPS intensities are given in Table 1. Except for *r* = 0.77, these ratios are closed to those obtained by bulk chemical determinations which indicates a homogeneous composition of the mixed catalysts. For the *r* = 0.77 sample, the difference between the bulk composition and that from XPS may indicate a heterogeneity of the sample. The sulfur to metal atomic ratios are higher than the expected stoichiometries in RuS_2 or $Ni_xRu_{1-x}S_2$ and NiS, or even NiS_2. The excess of sulfur is comparable to the values reported earlier (*7*, *8*), and it is

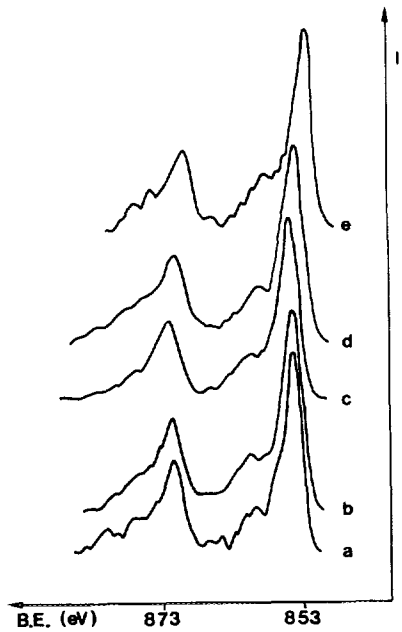

FIG. 4. Ni $2p_{1/2}$ and Ni $2p_{3/2}$ spectra of the sulfided NiRu catalysts: (a) NiRu(0.14), (b) NiRu(0.35), (c) NiRu(0.50), (d) NiRu(0.77), and (e) NiRu(1.0).

attributed to sulfur associated with the carrier on one hand, and on the other hand to extra sulfur on the surface of the crystallites (*12*). The results obtained from XPS chemical shifts and semiquantitative analysis are in general agreement with XRD, and they confirm that only one phase with a pyrite-like structure exists for the domain $0 \leq r \leq 0.77$.

Information about the distribution of the different elements is obtained by means of the ratios of Ru $3d_{5/2}$ or Ni $2p_{3/2}$ on Al $2p$. The variation of the intensity ratio Ru $3d_{5/2}$Al $2p$ versus the atomic Ru/Al composition in the bulk is given in Fig. 5. The graph shows an almost linear relationship between both variables for the NiRu samples with $r = 0.14, 0.35, 0.50$, and 0.77. The Ru sample alone does not follow the same trend, which indicates a different distribution of the Ru atoms on the support. An analogous linear tendency is observed for the Ni $2p_{3/2}$/Al $2p$ intensity ratio versus the bulk Ni/Al stoichiometry except for the Ni alone. Therefore, it is likely that the addition of a second element (Ru or Ni) improves the dispersion of the elements at the surface when compared with the single Ru/Al_2O_3 or Ni/Al_2O_3 sulfide catalysts.

Electron Microscopy

HREM micrographs of the sulfided NiRu(0.35) sample exhibit nearly spherical particles dispersed on the support. These pictures are similar to those previously observed and reported for the Ru/Al_2O_3 sulfided catalyst (*8*). In comparison to the Ru/Al_2O_3 sample sulfided under the same conditions (mean particle size 4.0 nm), the mean crystallite size of the NiRu(0.35) catalyst is lower (3.5 nm) and the size distribution is in a narrower range, indicating a bet-

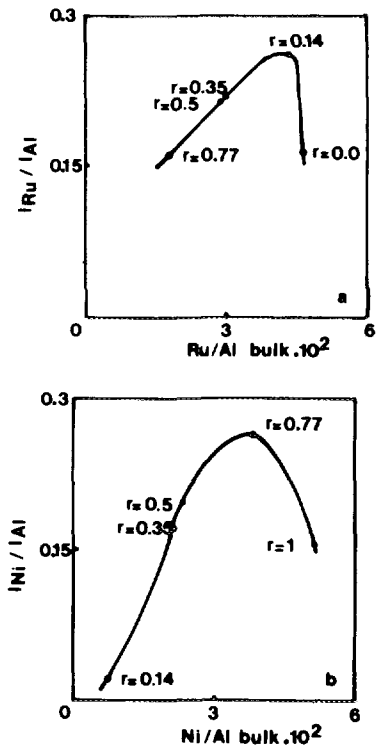

FIG. 5. XPS intensities ratio of the sulfided NiRu samples versus the atomic composition: (a) Ru $3d_{5/2}$/Al $2p$ and (b) Ni $2p_{3/2}$/Al $2p$.

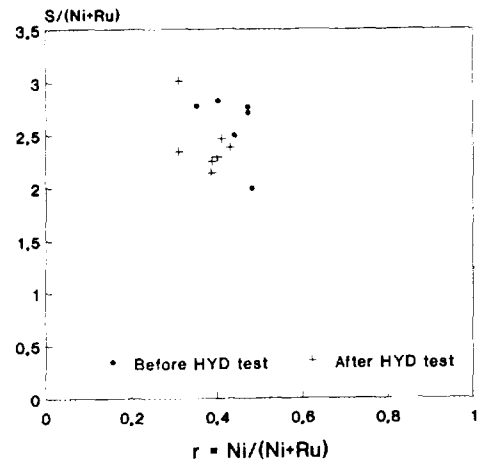

FIG. 6. STEM results for the NiRu(0.35) sample before (●) and after (+) catalytic testing. Sulfur on metal ratios versus atomic composition r = Ni/(Ni + Ru). Each point corresponds to one analyzed area.

ter dispersion on the surface. Up to now, no explanation is given to this observation.

STEM analysis of the NiRu(0.35) catalyst has been carried out before and after catalytic test at magnifications of 20×10^3 to 1×10^7 corresponding to areas of 3×10^3 nm^2 to 12 nm^2, respectively. Results reported in Fig. 6 indicate a good agreement with XPS data for the S/(Ni + Ru) ratio before test, and a decrease of the sulfur content after the reaction. After reaction, the slight excess of sulfur (compared to the stoichiometry S/Ru = 2) could be ascribed to remaining sulfur on the support. The various STEM analysis performed with different magnifications give values of the Ni/(Ni + Ru) ratios close to the theoretical one and no variations are observed after the reaction, which confirm that the initial solid solution is not significantly modified during the test.

TPR Measurements

Temperature-programmed-reduction profiles for the sulfided NiRu catalysts are given in Fig. 7. For $r < 0.77$ (also the same profiles are obtained for $r = 0.14$ and $r = 0.7$), the curves show very similar shapes with two apparent maxima at ca. 390 and 720 K. This shape is characteristic of the reduction of the pyrite structure of RuS_2 (*8*, *12*). This indicates that the pyrite structure of the solid solution is kept and also its stability is comparable to that of RuS_2. As concerns the TPR profiles for the NiRu(0.77) and NiRu(1.0) catalysts, broad bands with several apparent maxima are observed. These patterns are difficult to interpret, owing to the complexity of the transitions from sulfide to metal characteristics of nickel sulfides under the TPR conditions (*15*). However, it expresses the low stability of the rich nickel-containing mixed phase under the reducing conditions. That is, NiS_2 (or NiS) passes to the metallic state through several intermediate states, viz., NiS_{1-x}, Ni_3S_2, or Ni_9S_8.

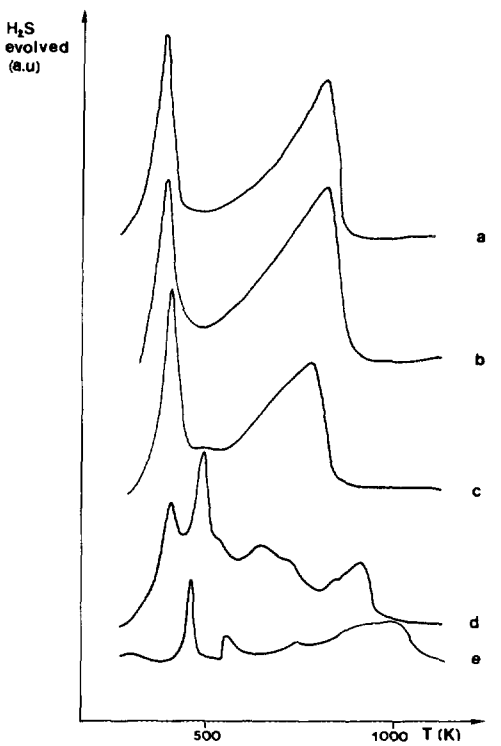

FIG. 7. TPR profiles for the sulfided NiRu samples: (a) NiRu(0.0), (b) NiRu(0.35), (c) NiRu(0.50), (d) NiRu(0.77), and (e) NiRu(1.0).

DISCUSSION

Characterization of Supported Ternary Sulfide Phases

In previous papers (*5*, *16*), we have shown that $Ni_xRu_{1-x}S_2$ solid solutions could be prepared in the whole range of composition, the evolution of the cell parameter determined from XRD spectra being in agreement with Vegard's law. These unsupported catalysts were stable in catalytic tests for composition up to 0.83, and their high hydrogenation activity was ascribed to the pyrite-type structure.

The supported state of this mixed phase is also characterized by a pyrite-type structure, as shown by XRD patterns. The lattice parameters are in agreement with the ones calculated for unsupported samples, showing the formation of NiRu solid solutions for compositions up to $r = 0.7$. This pyrite structure contains typically S_2^{2-} anions. XPS spectra recorded for the catalysts with r up to 0.5 exhibit S_{2p} maxima at a constant binding energy (162.8 ± 0.1 eV) corresponding to the disulfide polyanions. For $r = 0.77$, the pyrite phase still exists, but XPS also indicates the presence of some S^{2-} anions. Moreover, temperature reduction profiles obtained for catalysts with $r < 0.77$ are characteristic of the reduction of the RuS_2 pyrite structure. This indicates the similarity of the behaviour of these phases under reducing conditions. All of these physicochemical characterizations show that elements of the ternary nickel–ruthenium–sulfur solid solution have been synthesized on the support up to a composition near 0.7. The stability of these phases during the catalytic test is deduced from the STEM analysis performed on the catalysts before and after the reaction since the Ni/(Ni + Ru) ratio is maintained in a narrow range close to the chemical composition.

Electronic Properties of the Mixed Phase

There has been considerable interest in the electronic structure of the transition-metal dichalcogenides because of their wide range of physical properties. Among these materials, RuS_2 compound was largely studied. The electronic structure of the pyrite material RuS_2 was investigated by several authors by use of the self-consistent band structure calculations or the extended-Hückel method (*17*, *18*). All of them agree on the following results which provide also a general molecular orbital scheme of MS_2 pyrite structures (M = Fe, Co, Ni, Cu, and Zn). In this structure, each Ru^{2+} ion is surrounded by six S_2^{2-} molecules with the site symmetry represented by S_6. The octahedral component of the ligand field causes metal d levels to be splitted into triply degenerate t_{2g} and doubly degenerate e_g components. The t_{2g} and e_g degeneracies are removed by the strong octahedral crystal field of the S_2^{2-} ions. The t_{2g} orbitals orient themselves away from the Ru–S bonding directions and are essentially nonbonding. The e_g orbitals on the other hand, orient themselves along the Ru–S bonding directions and hybridize with S_{3p} levels. The hybridization occurs in such a way as to preserve the level structure of the S_{3p} bands of the hypothetical S_2^{2-} materials. The antibonding (Ru e_g^*)–(S_{3p} σ^*) hybrid states form conduction bands. In the case of NiS_2, this band is 50% filled (two electrons are added) and the phase behaves as a Mott semiconductor (*19*). For the $Ni_xRu_{1-x}S_2$ supported system with the same pyrite-type structure, as x increases, the (Ru e_g^*)–(S_{3p} σ^*) hybrid state is filled up to ca. 35%, corresponding to $x = 0.7$. An important change of these electronic properties can be expected for the $x = 0.5$ sample. In this case, the band is 25% filled and this compound would be isoelectronic with CoS_2, which is a metallic conductor (*19*). Therefore, Ni addition to Ru disulfide will induce the apparition of a metallic character first (25% of the conduction band filled for $x = 0.5$) and after, with increasing Ni content, a semiconductor behaviour.

Recently, infrared spectroscopy using CO as the probe molecule was used to characterize the adsorbant properties of this

$Ni_xRu_{1-x}S_2/Al_2O_3$ systems (*20*). A comparison of CO adsorption on NiRu catalysts with that of the unicomponent ones shows that the νCO wavenumber attributed to sulfided nickel is shifted to higher wavenumbers, and the intensity of this band presents a maximum at ca. $r = 0.5$. Nickel sulfide alone (NiS) adsorbs only a small amount of CO molecules. This indicates a deep change of the adsorbant properties of the surface nickel sites. Besides, the νCO wavenumber corresponding to ruthenium sulfide is not modified when nickel content increases, which suggests that the properties of ruthenium sites are less affected by the nickel proximity in the ternary phase than those of nickel sites.

Relevances to Catalytic Activity

The catalytic activity determinations show a 30-fold increase of the hydrogenation rates (see Fig. 1) for the $Ni_{0.5}Ru_{0.5}S_2$ supported sample in comparison to ruthenium sulfide alone. Both theoretical considerations and experimental CO chemisorption studies indicate deep change for this mixed phase stoichiometry. Undoubtly, the main change has to be ascribed to a nickel site in a pyrite surrounding. This new site present largely enhanced chemisorptive properties compared to nickel in pure nickel sulfides with different surroundings.

Moreover, it was shown recently that ruthenium sulfide present a particular ability for hydrogen activation (*21*). We can assume that this ability remains for the compounds of this ruthenium-sulfide-based solid solution. Both factors can cooperate to perform the hydrogenation reaction. This would explain the very large synergetic effect observed in this study.

However, for supported catalysts, the synergetic effect is several times higher than for unsupported ones (factor of 2). On that account, the carrier would play an important role by improving the dispersion of the active phase. As already mentioned for ruthenium sulfide on alumina, the formation of small particles induces some preferential exposed planes, favouring hydrogenation properties (*8*).

CONCLUSIONS

The members of the solid solution $Ni_xRu_{1-x}S_2$ supported over alumina have been prepared up to $x = 0.7$. This represents the first example of the transposition of a well defined ternary phase to the supported state. The physicochemical properties of these phases have been retained, as well as their exceptional hydrogenating properties.

ACKNOWLEDGMENTS

We are grateful to Dr. F. Beauchesne for the HREM measurements and to Mr. L. Gengembre for his help in the XPS experiments. J. A. De Los Reyes is indebted to the CONACYT (Mexico) for financial support.

REFERENCES

1. See, for instance, Weisser, O., and Landa, S., "Sulphide Catalysts, Their Properties and Applications." Pergamon Press, Oxford, 1973; Zdrazil, M., *Catal. Today* **3,** 269 (1988).
2. Pecoraro, T. A., and Chianelli, R. R., *J. Catal.* **67,** 430 (1981).
3. Lacroix, M., Boutarfa, N., Guillard, C., Vrinat, M., and Breysse, M., *J. Catal.* **120,** 473 (1989).
4. Passaretti, J., Chianelli, R. R., Wold, A., Dwight, K., and Covino, J., *J. Solid State Chem.* **64,** 365 (1986).
5. Vrinat, M., Lacroix, M., Breysse, M., Bellaloui, A., Mosoni, L., and Roubin, M., *in* "Proceedings, 9th International Congress on Catalysis, Calgary, 1988," (M. J. Philips and M. Ternan, Eds.), Vol. 1, p. 88. Chem. Inst. of Canada, Ottawa, 1988.
6. Vrinat, M., Lacroix, M., Breysse, M., Mosoni, L., and Roubin, M., *Catal. Lett.* **3,** 405 (1989).
7. De los Reyes, J. A., Göbölös, S., Vrinat, M., and Breysse, M., *Catal. Lett.* **5,** 17 (1990).
8. De los Reyes, J. A., Vrinat, M., Geantet C., and Breysse, M., *Catal. Today* **10,** 645 (1991).
9. Scofield, J. H., *J. Electron Spectrosc.* **8,** 129 (1976).
10. Nefedov, V. I., Sergushin, N. P., Band, I. M., and Trzhaskovskaya, M. B., *J. Electron Spectrosc.* **2,** 283 (1973).
11. Yuan, S., Decamp, T., Lacroix, M., Mirodatos, C., and Breysse, M., *J. Catal.* **132,** 253 (1991).
12. Geantet, C., Calais, C., and Lacroix, M., *C. R. Acad. Sci. Ser. II* **315,** 439 (1992).
13. Mitchell, P. C. H., Scott, C. E., Bonnelle, J. P. and Grimblot, J. G., *J. Catal.* **107,** 482 (1987).
14. van der Heide, H., Hemmel, R., van Bruggen, F. and Haas, C., *J. Solid State Chem.* **33,** 17 (1980).

15. Scheffer, B., Dekker, N. J. J., Mangnus, P. J., and Moulijn, J. A., *J. Catal.* **121,** 18 (1990).
16. Bellaloui, A., Mosoni, L., Roubin, M., Vrinat, M., et Lacroix, M., *C. R. Acad. Sci. Paris Ser. C* **307,** 1171 (1988).
17. Holzwarth, N. A. W., Harris, S., Liang, K. S., *Phys. Rev. B* **32,** 3745 (1985).
18. Huang, Y. S., and Chen, Y. F., *Phys. Rev. B.* **38,** 7997 (1988).
19. Bullet, D. W., *J. Phys. C: Solid State Phys.* **15,** 6163 (1982).
20. De Los Reyes, J. A., Vrinat, M., Breysse, M., Maugé, F., and Lavalley, J. C., *Catal. Lett.* **13,** 213 (1992).
21. Lacroix, M., Mirodatos, C., Breysse M., Decamp, T., and Yuan, S., Preprint, 10th International Congress on Catalysis 19–24 July 1992, Budapest, Hungary, oral paper 34.